# The effect of graphite number per area on tribological behavior of high-strength compacted cast irons in lubricated tests

Giuseppe Pintaude [1]* ©
Daniella Wollmann [1] ©

## Abstract

Compacted graphite irons (CGIs) are considered a suitable option for heavy-duty engine blocks against grey cast irons due to their superior mechanical, thermomechanical, and tribological properties. Even though a large number of studies exist, high-strength CGIs still need more investigations related to the correlation between their microstructure and tribological performance. This study aims to investigate the effect of graphite number per area on friction and wear of two CGI grades - GJV450 and GJV500 - under lubricated ring-on-cylinder tests. The lubricant used was SAE CF-30 at 40 °C and the load was 75 N. Roughness measurements, scanning electron microscope, and electron dispersive spectrometry was performed to identify the differences in tribological behavior. The wear performance was evaluated using the variation on structure height S3k (=Spk+Sk+Svk). Any difference was determined for both cast irons in terms of coefficient of friction but the GJV450 presented a more intense plastic deformation, resulting in a higher variation of the S3k factor. Therefore, the reduction in graphite number per area affected the wear performance, justifying the preferential use of GJV500.

**Keywords:** Compacted graphite iron; Lubricated wear; Heavy-duty engine blocks.

## 1 Introduction

Cast irons are widely used for engine blocks in heavy-duty applications due to their good combination between thermo-mechanical fatigue and machinability. Compacted graphite iron (CGI) has been calling attention because of its better performance when compared to grey cast iron. In CGI the graphite particles are connected forming a "coral-like" shape, leading to superior mechanical properties, including the reduction of both nucleation and propagation of cracks [1] and improved thermomechanical fatigue behavior. The CGI showed better performance than grey cast iron under lubricated [2] and scratching [3] conditions.

However, the hardness of typical counterbody – piston rings – is in most cases much higher than the cast iron hardness, even for CGI [4]. In this sense, different strategies have been used to improve even more the mechanical properties. Among them, we can cite the austempering heat treatment [5,6], combined surface treatments [7], shallow nitriding [8], induction hardening [9], and the addition of alloying elements [10] are also good options that have been studied to improve the surface properties of graphite irons.

A new grade of CGI – GJV500 – has been introduced [11] by changing the graphite morphology. A remarkable result in terms of thermo-mechanical fatigue was described by Bon et al. [12] for this new grade, which presented a 150% increase in fatigue life when compared to GJV450. The authors found that the graphite structure in the eutectic cell of

GVJ500 changes from worm to round shape at the graphite boundaries, imposing more difficulties to propagate cracks.

In terms of tribological response, compacted graphite iron (GJV450) performed better than gray cast iron under lubricated conditions [13]. However, under severe contact conditions (boundary lubrication), the performance of GJV500 was not much superior to that presented by GJV450 [14]. Within this context, this study aims to compare the effect of graphite number per area of CGI grades GJV450 and GJV500 assessed with lubricated ring-on-cylinder tests.

## 2 Experimental procedures

Two engine blocks of high-strength CGI grades were manufactured. Table 1 presents their chemical compositions. Figure 1 shows the etched microstructures, where compacted graphite can be seen with some nodules. Most of the metallic matrix is composed by pearlite. Some ferrite can be identified associated with graphite nodules.

The hardness of the metallic matrix was determined through two approaches: Vickers microhardness (100 g load) and nanoindentation (450 mN load). Both techniques resulting in quite similar values, as shown in Figure 2. By opposing, the global hardness measured through the Brinell scale showed that higher hardness GJV500 is harder than GJV450, which

[1]Laboratório de Superfícies e Contato, LASC, Departamento Acadêmico de Mecânica, Universidade Tecnológica Federal do Paraná, UTFPR, Curitiba, PR, Brasil.
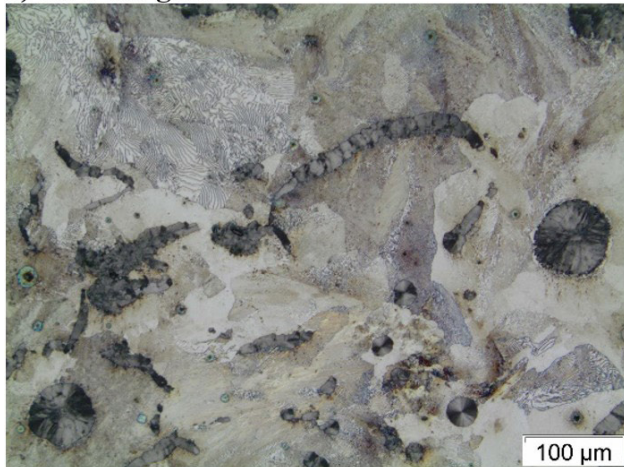
*Corresponding author: pintaude@utfpr.edu.br

**Table 1.** Chemical composition of CGIs (wt%)

| Element | | | | | | | | | | | | |
|---|---|---|---|---|---|---|---|---|---|---|---|---|
| CGI grade | *Ceq | Si | Mn | P | Cr | Cu | W | Sn | Mg | Ce | Zn | La |
| GJV450 | 4.40 | 2.25 | 0.34 | 0.03 | 0.03 | 2.12 | 0.03 | 0.10 | 0.02 | 0.03 | 0.12 | 0.02 |
| GJV500 | 4.50 | 2.26 | 0.34 | 0.02 | 0.05 | 2.16 | 0.12 | 0.10 | 0.04 | 0.08 | 0.10 | 0.03 |

*Ceq is the equivalent carbon.

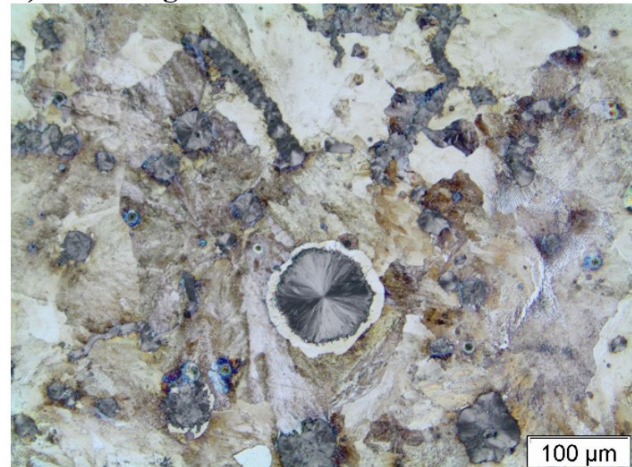**a) GJV450 grade**



**b) GJV500 grade**
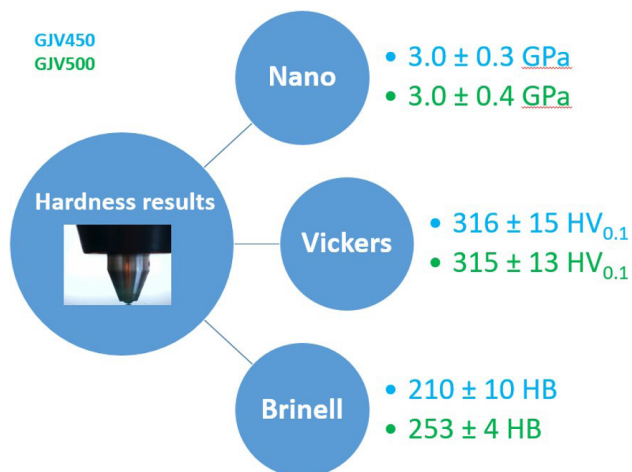


**Figure 1.** Microstructures of CGIs.



**Figure 2.** Hardness results of CGIs.

is expected according to these CGI grades [15]. Therefore, the changes promoted in the graphite morphology are the key to explain these results.

Elastic moduli determined using nanoindentation for GJV450 and GJV500 were $150 \pm 12$ and $147 \pm 16$ GPa, respectively. These results are in the range of elastic modulus indicated in ISO 16112:2017 [15].

Graphite count was performed on images without chemical attack (Figure 3). The average values correspond to a series of twelve images with 100x magnification.

The criteria for the graphite count were considering ISO 16112:2017 [15]. A summary of the results is presented in Figure 4. The graphite number per area was higher for GVJ450. These results agree with this softer cast iron. More graphite nodules are identified in GJV500 (Figure 3b), associated with higher magnesium and cerium percentages in the composition [16]. Nodularity was determined following the same methodology as Domeij et al. [17].

The engine blocks were honed in a two-step process for obtaining plateau finishing: the first step was the roughening and the second one the finishing. More details about honing processing can be found elsewhere [13]. The cylinders were machined to reach 105 mm diameter. Then they were cut into small pieces and machined into specific dimensions (8.3 x 10.1 x 24 mm) to get samples. The samples are placed in a holder (Figure 5). Its cavity is filled with lubricant oil, covering the sample surface completely. The heating of lubricant is achieved using a resistance inside the holder.

The used counterbody was a segment of industrial piston ring with an asymmetric profile (83 mm nominal diameter and 1.2 mm thickness). It is martensitic stainless steel, nitrided at its contact surface. The Vickers hardness of its compound layer is about $1,100 \; HV_{0.1}$ [13].

Tribological behavior was assessed using a CETR UMT-2 reciprocating module. The testing parameters are described in Table 2. Tests were repeated three times for both tested materials. Coefficients of friction (COF) were obtained with the average values of up and down semi-cycles with a data acquisition rate of 100 Hz.
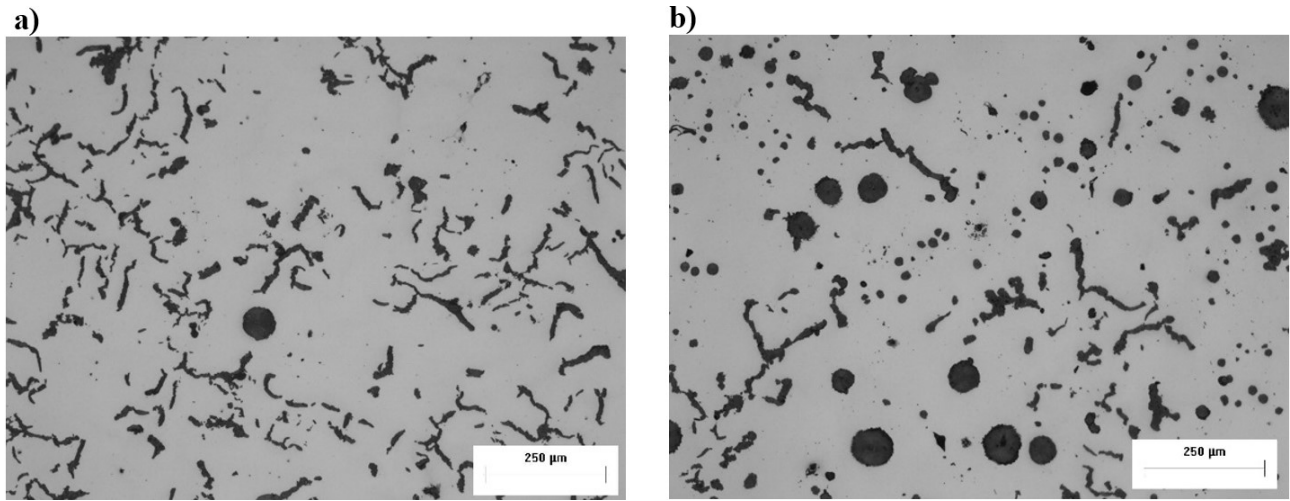
a)

b)



**Figure 3.** Optical microscopy images used for graphite count of CGIs: (a) GJV450; and (b) GJV500.
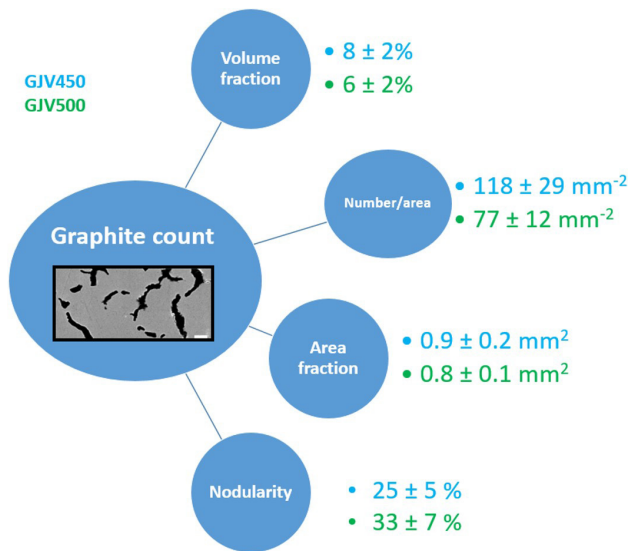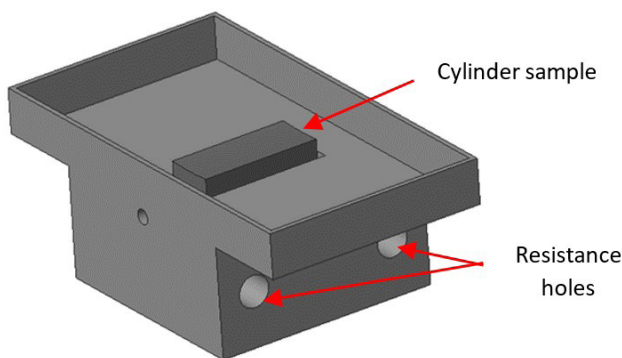


**Figure 4.** Graphite count of CGIs.



**Figure 5.** Cylinder sample holder.

Surface roughness measurements were evaluated using an optical interferometer Talysurf CCI Lite – Taylor Hobson, with a resolution of 1024 x 1024 pixels. The measurement area

**Table 2.** Parameters used in ring-on-cylinder test

| Variable | Value |
|---|---|
| Normal load [N] | 75 |
| Frequency [Hz] | 5 |
| Lubricant | Petronas Urania SAE 30 CF |
| Temperature [°C] | 40 |
| Testing time [h] | 4 |

was $0.8 \times 0.8$ mm$^2$ and ten measurements were performed in each sample before and after the tribo-tests. Initial surfaces have plateau finishing, and, after the tests, worn regions associated with the mid-stroke were measured.

To estimate the level of plastic deformation, the plasticity index was calculated according to Equation 1.

$$\psi = \frac{E^*}{H}\left(\frac{\sigma_{Zs}}{\beta}\right)^{1/2} \quad (1)$$

where:

$E^*$ is the combined elastic modulus [GPa];

$H$ the macrohardness of the softer material [GPa];

$\sigma_{Zs}$ is the height standard deviation of summits [μm]; and

$\beta$ is the mean radius of summits [μm].

The 3D images from interferometry were used as input in the Mahle-Summits program [18] to obtain the parameters $\sigma_{Zs}$ and $\beta$.

Determining wear is difficult, especially when almost zero wear is present. The wear rates are usually obtained using the variations in surface roughness to solve this issue. Unfortunately, there is not consensual conclusion given in the literature about the roughness parameters used for this analysis. Here, the methodology used to evaluate the low-wear was based on the variation in the structure height S3k (= Spk+Sk+Svk), before and after wear testing, as used previously in similar researches [6,14,19]. Threshold filtering of 1% was used in roughness measurements. This filter

disregards the percentage of extreme values for the structure height parameters as an attempt to minimize the problems pointed out previously about S3k [20]. In this fashion, the S3k methodology was applied in a comparative way. If the error was considered significant, it would be the same for all cases, which means that the comparison still remains valid.

The worn surfaces were analyzed using a Zeiss EVO-MA15 scanning electron microscope (SEM). The electron dispersive spectroscopy (EDS) technique was used on worn regions to characterize the presence of tribofilms, measuring Zn, P, and S.

## 3 Results

### 3.1 Friction behavior and local chemical analysis

The average coefficient of friction after 4 hours was $0.11 \pm 0.02$ for both CGIs. Also, the film parameter was 0.6, which corresponds to the boundary lubrication regime. In previous research conducted in the same testing conditions, do Vale et al. [2] found similar COF for GJV450, although under different lubrication regimes. In that case, the film parameter characterized mixed lubrication, resulted from different original surface roughness of samples. It is important to highlight that the differences in test configuration and initial surface conditions could bring conflicting results.

Worn surfaces were observed through SEM images (Figure 6) and EDS was used to detect the presence of Phosphorous, Sulfur, and Zinc after reciprocating tests. These elements can indicate the formation-removal-formation mechanisms of ZDDP tribofilms, reported previously [19]. EDS measurements were performed on the plateaus (measurements 1 and 2) and in the grooves (measurement 3). It is possible to verify that inside the grooves there was no formation of ZDDP because in these regions there was not enough mechanical contact.

On the other hand, measurements performed on the plateaus showed the presence of ZDDP elements. There were some regions that not all the elements of ZDDP were found in the same measurement. This result was also found by do Vale et al. [13] even for longer tests. These variations can be attributed to the successive formation and removal of tribofilms during the tests, showing the non-continuity of ZDDP.

With the sum of the percentage of ZDDP elements seen in Figure 6, it is easier to verify that the tribofilm formation was more intense for GJV450, which is related to the higher level of deformation that happened in this material. Other investigations [7,14,19] showed a higher sum of (Zn+P+S), meaning that in the current investigation the formation of tribofilms was not significant to determine the average COF values. For example, Wollmann et al. [6] determined 10% of (Zn+P+S) for rings manufactured in austempered CGI, while the same authors [14] verified almost the same value for GJV450 using 170N load for cylinder samples.
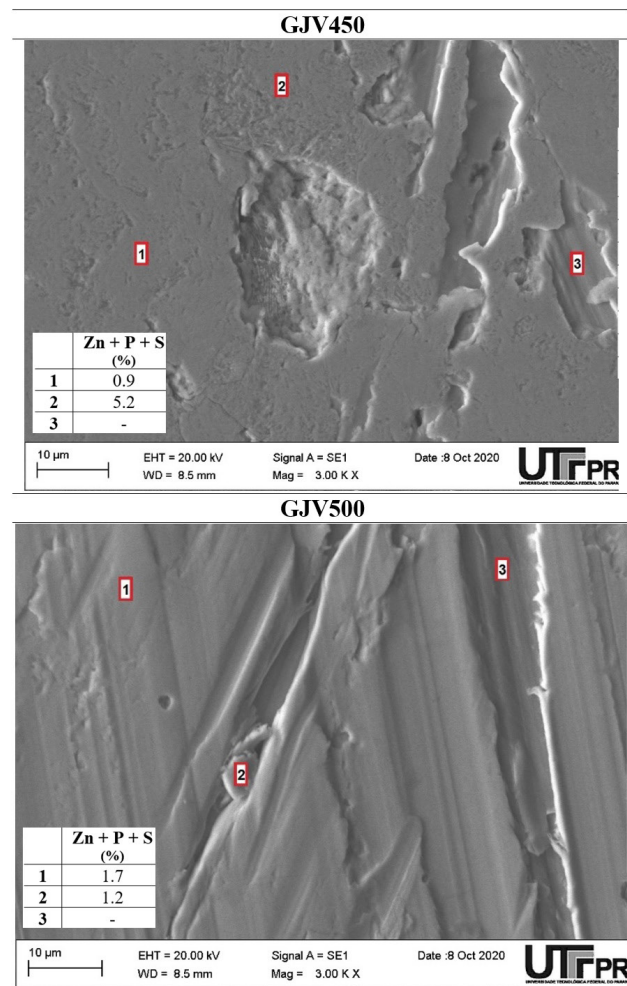


**Figure 6.** Local chemical analysis by EDS of worn surfaces. The sum of (Zn+P+S) is also indicated.

In the next section, the features related to the deformation of both CGIs during the tribo-tests will be more explored.

### 3.2 Surface deformation and wear performance

Surface roughness evaluation before and after tribo-tests are shown in Table 3. It is possible to verify the reduction in the Sq parameter, indicating the flattening of surfaces after the tests. The result was more significant for GJV450, which reduced 20%, while GJV500 reduced 6%. Sk parameter also reduced, agreeing with the flattening indicated by the reduction of Sq.

Spd and Spc hybrid parameters also reduced significantly after the tests for both materials, indicating the tendency of reduction in asperities density and radius, respectively.

Sku and Ssk are known as sensible parameters, presenting great dispersion [21]. The variation is better represented by images of height distribution curves shown in Figure 7. These curves are representative, illustrating the behavior independently from the average and standard deviation. Is it clear the shift and higher concentration of
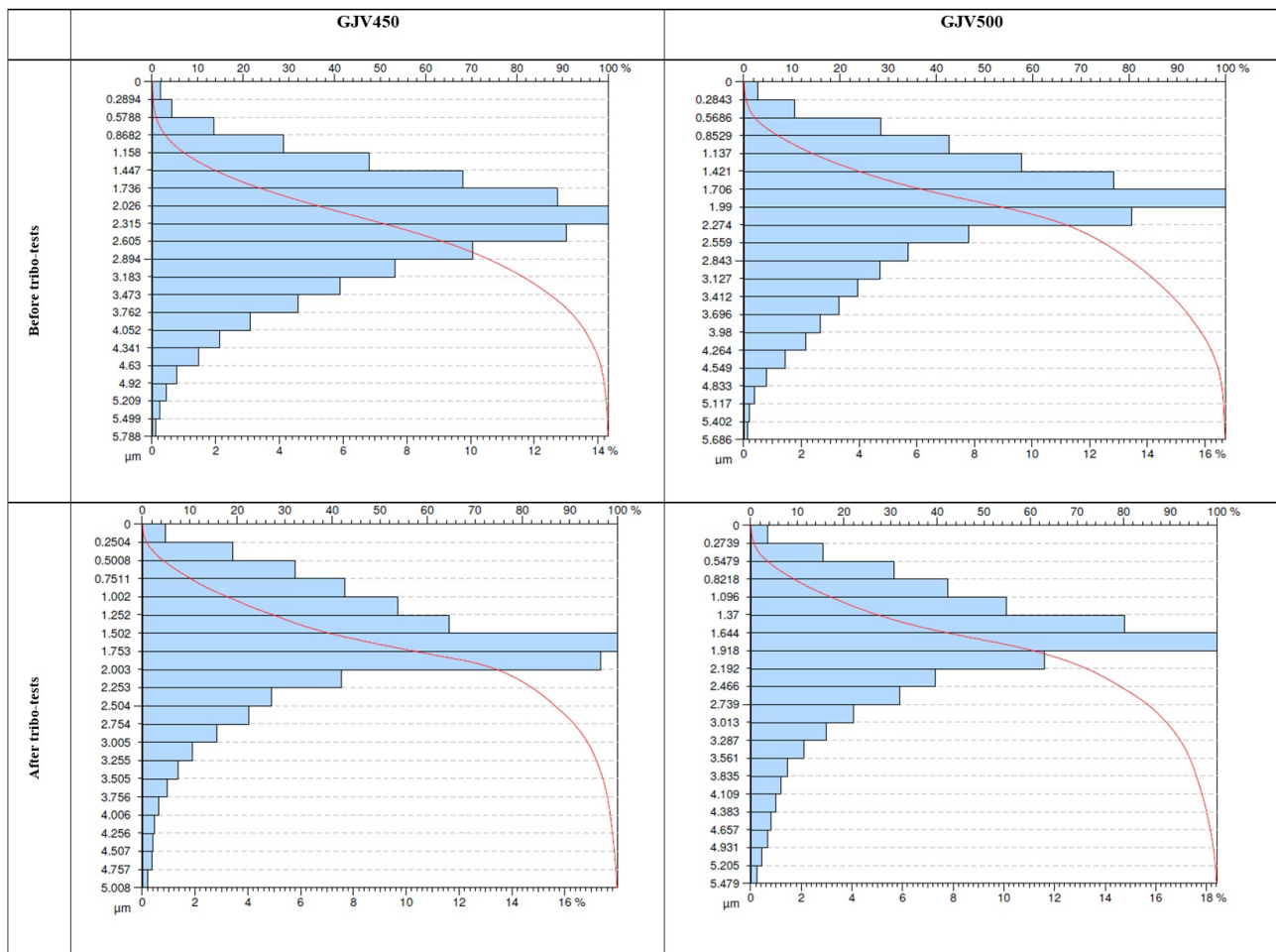
**Figure 7.** Comparison of height distribution curves for CGIs before and after tribo-tests.

**Table 3.** Roughness parameters of honed surfaces before and after tribo-tests

| CGI | Condition | Sq (µm) | Ssk (-) | Sku (-) | Spk (µm) | Sk (µm) | Svk (µm) | Spd (mm⁻²) x10³ | Spc (mm⁻¹) x10³ |
|---|---|---|---|---|---|---|---|---|---|
| **GJV450** | **Before** | 0.9 (±0.1) | -0.8 (±0.3) | 4.1 (±1.0) | 0.6 (±0.1) | 1.8 (±0.2) | 1.5 (±0.3) | 63.8 (±1.3) | 0.61 (±0.04) |
| | **After** | 0.7 (±0.1) | -0.7 (±0.4) | 5.0 (±1.0) | 0.6 (±0.1) | 1.3 (±0.1) | 1.3 (±0.2) | 26.1 (±2.6) | 0.28 (±0.01) |
| **GJV500** | **Before** | 0.9 (±0.1) | 1.0 (±0.2) | 4.6 (±1.0) | 0.6 (±0.1) | 1.8 (±0.2) | 1.6 (±0.2) | 65.4 (±2.8) | 0.74 (±0.05) |
| | **After** | 0.9 (±0.1) | -1.0 (±0.3) | 5.0 (±0.9) | 0.6 (±0.1) | 1.5 (±0.1) | 1.6 (±0.3) | 27.1 (±3.1) | 0.29 (±0.01) |

the distribution in both materials after the tribo-tests. This is typical behavior of honed surfaces after wear tests and was already described by Jeng et al. [22].

Considering metallurgical aspects of the CGIs, GJV500 presented not only higher nodularity but also less number of graphite per area than GJV450. This contributed to the slightly smaller plasticity index for GJV500, as shown in Table 4. However, all values are much higher than 1, meaning that both materials will be exposed to intense plastic deformation.

Hypothesis testing was performed using the results of plasticity indexes for both materials before and after the tests, according to Table 4. It was considered as a null hypothesis that the average of both populations should be equal. Student's t-distribution was used considering a 95%

**Table 4.** Plasticity index ($\psi$) calculated before and after wear tests

| Material | Condition | $\sigma_{Zs}$ (µm) | $\beta$ (µm) | $\psi$ (-) |
|---|---|---|---|---|
| **GJV450** | Before | 0.50 ± 0.04 | 8.9 ± 0.9 | 9.7 ± 0.7 |
| | After | 0.42 ± 0.04 | 15.5 ± 1.7 | 6.8 ± 0.6 |
| **GJV500** | Before | 0.49 ± 0.02 | 7.0 ± 1.0 | 11.0 ± 1.0 |
| | After | 0.42 ± 0.02 | 17.3 ± 1.8 | 6.1 ± 0.4 |

of the confidence interval. For both conditions (before and after tests) the null hypothesis was discarded, indicating that the average of populations is different between each other.

SEM images confirmed the flattening of surfaces and it is possible to verify that GJV450 presented more deformation (Figure 8). This result agrees with the more
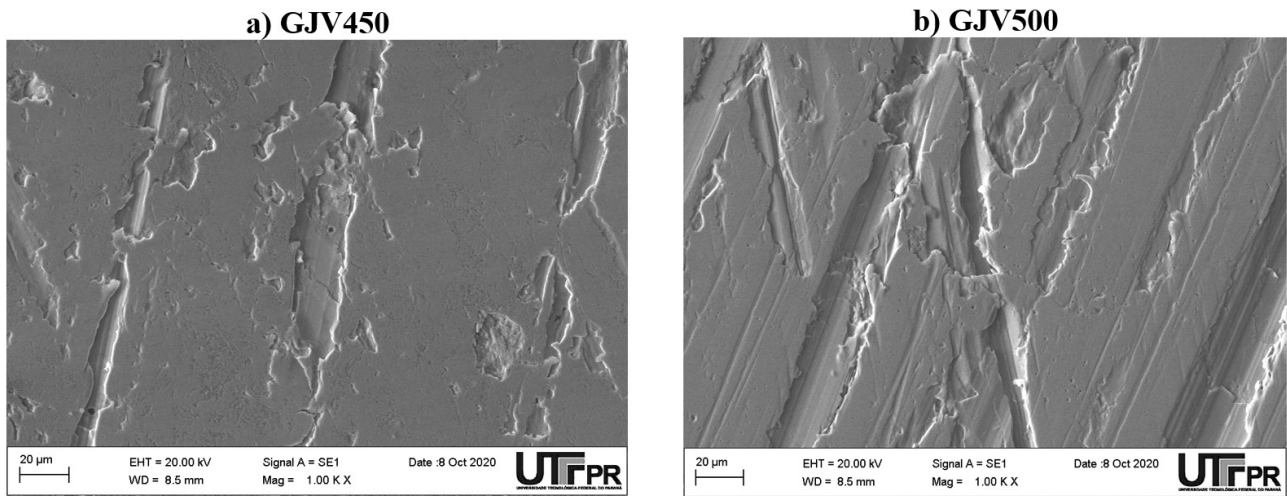
### a) GJV450

### b) GJV500



**Figure 8.** Honed surfaces of CGIs after tribotests.
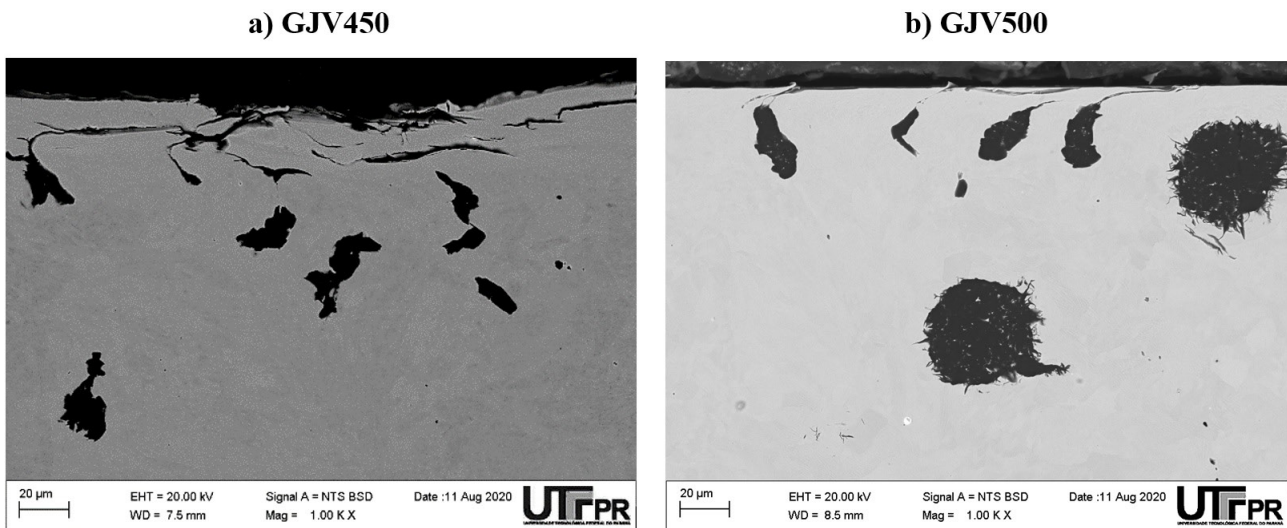
### a) GJV450

### b) GJV500



**Figure 9.** Transversal sections of worn surfaces of CGIs.

expressive reduction of the Sq and Sk parameters for this material. These results are also described by Truhan et al. [23], showing that more severe loads can keep deforming surfaces until a polished condition be achieved.

Plastic deformation of worn surfaces is revealed in cross-sectional images of mid-strokes (Figure 9). More intense damage is verified for GJV450 cast iron in comparison to GJV500. It is also possible to see cracks nucleating in subsurface graphites towards the surface. This phenomenon contributes to the ejection of graphites, also described by Hase [24] for grey and nodular cast irons and observed by Wollmann and Pintaude [14] for the same grades of CGI used in this study.

Friction behavior is a combination of multiple interactions between tribo-elements. In reference [7] three significant aspects for friction were discussed, to explain a

compensating effect that resulted in similar values: i) plastic deformation, ii) ejection of graphites, and iii) tribofilm formation. Considering the sum (Zn+P+S) as indicative of tribofilm formation, this aspect can be considered less significant, as previously discussed. Therefore, the level of plastic deformation and the possible ejection of graphites play a decisive role to define the friction. One can see in Figure 9 that the more the deformation, the more the ejection of graphites. In this way, there is a compensating effect between deformation and the presence of graphites at the contact area.

Defining wear rate under lubricated conditions is not a simple task. Fernandes et al. [19] estimated the wear using the changes in k parameters (%ΔS3k) of Abbott-Firestone curves (Figure 7). Based on this approach, in a previous study with similar materials but using higher

load and oil temperature, GJV500 performed better than GJV450 [14]. The same is verified here, being the ΔS3k 16 and 6% for GJV450 and GJV500, respectively. It means a better tribological performance of GJV500.

Here, the GJV450 cast iron presented more number of graphite per area. This is the most significant microstructural aspect defining the topographical changes that occurred during the lubricated tests. When nodular graphite was put in contact with the stylus profilometer, graphite areas were scratched [25]. It means that the elastic contact area changed significantly without the presence of graphite areas. Therefore, the strategy to modify this microstructural aspect is effective to improve the tribological behavior under lubricated conditions.

Another strategy is to enhance the hardness of the pearlitic matrix, as described by Lacaze et al. [26]. These authors detected an intriguing dispersion on microhardness values for CGI containing 1.28% Cu. The range of values was 250-475 HV exclusively for the pearlitic matrix, which certainly would affect the tribological responses. This should consider a potential next move to verify the tribological performance under lubricated conditions.

## 4 Conclusions

Lubricated ring-on-cylinder tests were performed in two high-strength CGI grades (GJV450 and GJV500). Based on the discussed results, the following considerations can be drawn:

- The coefficient of friction results obtained after the four hours of tests was the same for both cast iron grades. The friction behavior was determined by a compensating effect between plastic deformation and ejection of graphites; and

- The reduction of graphite number per area reduced the wear estimated using changes of structure height.

## References

1 Guesser W, Schroeder T, Dawson S. Production experience with compacted graphite iron automotive components. AFS Trans. 2001;109:1-11.

2 Vale JL, Guesser WL, Silva CH, Pintaúde G. Evaluation of friction coefficient of lamellar and compacted graphite irons in lubricated ring-on-cylinder system. Warrendale: Society of Automotive Engineers; 2018. (SAE Technical Paper; no. 2018-36-0058).

3 Vale JL, Cortz M, Bertolini VM, Silva CH, Pintaude G. Comparison of scratch resistance of lamellar and compacted graphite irons used in cylinder liners. Journal of the Brazilian Society of Mechanical Sciences and Engineering. 2017;39(10):3981-3988.

4 Mehran QM, Fazal MA, Bushroa AR, Rubaiee S. A critical review on physical vapor deposition coatings applied on different engine components. Critical Reviews in Solid State and Materials Sciences. 2017;43:158-175.

5 Ghasemi R, Hassan I, Ghorbani A, Dioszegi A. Austempered compacted graphite iron: influence of austempering temperature and time on microsctructural and mechanical properties. Materials Science and Engineering A. 2019;767:138434.

6 Wollmann D, Pintaude G, Ghasemi H. Effect of austempering treatment on lubricated sliding contact of compacted graphite iron. SN Applied Sciences. 2020;2(12):1947.

7 Writzl V, Rovani AC, Pintaude G, Lima MSF, Guesser WL, Borges PC. Scratch resistances of compacted graphite iron with plasma nitriding, laser hardening, and duplex surface treatments. Tribology International. 2020;143:106081.

8 Santos D Fo, Tschiptschin AP, Goldenstein H. Effects of plasma nitriding on the surface topography of gray cast iron specimens. Surface and Coatings Technology. 2020;404:126464.

9 Slatter T, Lewis R, Jones AH. The influence of induction hardening on the impact wear resistance of compacted graphite iron (CGI). Wear. 2011;270(3-4):302-311.

10 Lyu Y. Abrasive wear of compacted graphite cast iron with added tin. Metallography, Microstructure, and Analysis. 2019;8(1):67-71.

11 Guesser WL, Martins LP. Stiffness and vibration damping capacity of high strength cast irons. Warrendale: Society of Automotive Engineers; 2016. (SAE Technical Papers; no. 2016-36-0126).

12 Bon DG, Ferreira MH, Bose WW Fo, Guesser WL. Fracture micromechanisms evaluation of high-strength cast irons under thermomechanical fatigue conditions. International Journal of Metalcasting. 2020;14(3):696-705.

13 Vale JL, Silva CH, Pintaude G. Tribological performance assessment of lamellar and compacted graphite irons in lubricated ring-on-cylinder test. Wear. 2019;426-427:471-480.

14 Wollmann D, Pintaude G. Tribological performance of high-strength cast iron in lubricated contact containing carbon black. Wear. 2021;476:203743.

15 International Organization for Standardization. ISO 16112:2017: compacted (vermicular) graphite cast irons: classification. Geneva: ISO; 2017.

16 Alonso G, Stefanescu DM, Larrañaga P, Suarez R. Graphite nucleation in compacted graphite cast iron. International Journal of Metalcasting. 2020;14(4):1162-1171.

17 Domeij B, Hernando JC, Diószegi A. Size distribution of graphite nodules in hypereutectic cast irons of varying nodularity. Metallurgical and Materials Transactions. B, Process Metallurgy and Materials Processing Science. 2018;49(5):2487-2504.

18 Tomanik E. Modelling of the asperity contact area on actual 3D surfaces. Warrendale: Society of Automotive Engineers; 2005. (SAE Technical Papers; no. 2005-01-1864).

19 Fernandes W, Tomanik E, Moreira H, Cousseau T, Pintaude G. Effect of aged oils on ring-liner wear. SAE International Journal of Fuels and Lubricants. 2020;13(2):167.

20 Obara RB, Sinatora A. Quantification of cylinder bores almost 'zero-wear'. Wear. 2016;364-365:224-232.

21 Dong WP, Sullivan PJ, Stout KJ. Comprehensive study of parameters for characterising three-dimensional surface topography: III: Parameters for characterising amplitude and some functional properties. Wear. 1994;178(1-2):29-43.

22 Jeng YR, Lin ZW, Shyu SH. Changes of surface topography during running-in process. Journal of Tribology. 2004;126(3):620-625.

23 Truhan JJ, Qu J, Blau PJ. A rig test to measure friction and wear of heavy duty diesel engine piston rings and cylinder liners using realistic lubricants. Tribology International. 2005;38(3):211-218.

24 Hase A. Visualization of the tribological behavior of graphite in cast iron by in situ observations of sliding interfaces. Tribology International. 2019;138:40-46.

25 Pintaude G, Brunetti C, Leite MV, Montanez-Calao LF. Effect of surface finishing on the elastic contact area evaluation of austempered ductile iron. Lubrication Science. 2013;25(2):101-109.

26 Lacaze J, Moussa C, Thebault Y, Guesser W. Extrema of micro-hardness in fully pearlitic compacted graphite cast iron. International Journal of Cast Metals Research. 2020;33(4-5):218-225.